International Journal of Pharmaceutics 663 (2024) 124536

Contents lists available at ScienceDirect

International Journal of Pharmaceutics

journal homepage: www.elsevier.com/locate/ijpharm

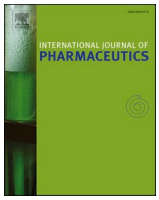

Leveraging 3D-printed microfluidic micromixers for the continuous manufacture of melatonin loaded SNEDDS with enhanced antioxidant activity and skin permeability

Baris Ongoren [a], Aytug Kara [a], Luca Casettari [b], Mattia Tiboni [b], Aikaterini Lalatsa [c], Amadeo Sanz-Perez [d], Elena Gonzalez-Burgos [d], Alejandro Romero [e], Antonio Juberías [f], Juan J. Torrado [a,g,*], Dolores R. Serrano [a,g,**]

[a] Department of Pharmaceutics and Food Technology, School of Pharmacy, Complutense University of Madrid, 28040 Madrid, Spain
[b] Department of Biomolecular Sciences, School of Pharmacy, University of Urbino Carlo Bo, Piazza del Rinascimento 6, 61029 Urbino, Italy
[c] Cancer Research UK Formulation Unit, School of Pharmacy and Biomedical Sciences, Robertson Wing, University of Strathclyde, 161, Cathedral Street, Glasgow G4 0RE, Scotland, UK
[d] Department of Pharmacology, Pharmacognosy and Botany, Faculty of Pharmacy, Complutense University of Madrid, Madrid, Spain
[e] Department of Pharmacology and Toxicology, School of Veterinary, Complutense University of Madrid, 28040 Madrid, Spain
[f] Dirección de Sanidad del Ejército del Aire, Princesa 87, 28008 Madrid, Spain
[g] Institute of Industrial Pharmacy Complutense University of Madrid, 28040 Madrid, Spain

ARTICLE INFO

Keywords:
Melatonin
SNEDDS
Topical administration
Antioxidant
Chemical weapons
3D printing
Microfluidic chips
Continuous manufacture

ABSTRACT

Vesicants are chemical warfare agents (CWAs) capable of causing severe skin damage and systemic toxicity. Melatonin, known for its anti-inflammatory and antioxidant properties, can mitigate the effects of these agents. Self-nano-emulsifying drug delivery systems (SNEDDS) containing a high melatonin concentration (5 %, 50 mg/g) were optimized using a quality-by-design approach from biocompatible, non-irritant excipients with a particle size of about 100 nm. The melatonin-loaded SNEDDS showed a 43-fold greater permeability than a conventional melatonin cream. Chemical stability at ambient temperature (25 °C) was maintained for one year. The preparation of optimised melatonin-loaded SNEDDS using a simple mixing method was compared to microfluidic micromixers. Mixing was successfully achieved using a 3D-printed (fused deposition modeling or stereolithography) T-shaped toroidal microfluidic chip (with a channel geometry optimized by computational fluid dynamics), resulting in a scalable, continuous process for the first time with a substantial reduction in preparation time compared to other conventional mixing approaches. No statistically significant differences were observed in the key quality attributes, such as particle size and melatonin loading, between mixing method till kinetic equilibrium solubility is reached and mixing using the 3D-printed micromixers. This scalable, continuous, cost-effective approach improves the overall efficiency of SNEDDS production, reduces the cost of quality control for multiple batches, and demonstrates the potential of continuous microfluidic manufacture with readily customizable 3D-printed micromixers at points of care, such as military bases.

1. Introduction

Melatonin is an indoleamine used widely to restore sleeping disorders at low doses, commonly at doses below 2 mg per day (Garfinkel et al., 1995). In recent years, the potential of melatonin beyond managing insomnia is linked to its ability to neutralize the oxidative stress of toxic substances, modulate the inflammatory response, and prevent DNA damage (Pandi-Perumal et al., 2006). However, much higher concentrations are required to elicit these effects, and thus, there is a need for products containing much greater concentrations than those currently available in marketed products. A study demonstrated that daily administration of melatonin at 10 mg/kg reduces oxidative stress and enhances DNA protection in diabetic rats (Sekkin et al., 2015). Doses of 20 mg/kg of melatonin were reported to substantially reduce

* Corresponding author at: Department of Pharmaceutics and Food Technology, School of Pharmacy, Complutense University of Madrid, 28040 Madrid, Spain.
** Corresponding author at: Institute of Industrial Pharmacy Complutense University of Madrid, 28040 Madrid, Spain.
E-mail addresses: torrado1@ucm.es (J.J. Torrado), drserran@ucm.es (D.R. Serrano).

https://doi.org/10.1016/j.ijpharm.2024.124536
Received 5 May 2024; Received in revised form 25 July 2024; Accepted 26 July 2024
Available online 27 July 2024

cyclophosphamide-induced genotoxicity in mice, fully normalizing bone marrow cell ratios (Shokrzadeh et al., 2014).

Vesicants represent a class of chemical warfare agents (CWAs) encompass various compounds such as mustards (including sulfur mustards and nitrogen mustards), lewisite (arsenical mustard), and phosgene oxime (classified as an urticant and corrosive agent despite its vesicant categorization) and are responsible for inducing blistering (vesicles) while they impact the respiratory tract differently. Mustards primarily target the large airways as type 1 agents, while phosgene oxime affects the lower airways and alveoli as a type 2 agent, and lewisite demonstrates characteristics of a mixed agent (Cruz-Hernandez et al., 2022). Vesicant CWAs are used in military conflicts (Romero et al., 2021), and the first clinical signs and symptoms after exposure appear between 2–48 h, depending on exposed dose, temperature, humidity, region, and exposed body area. The respiratory tract, eyes, and skin are the most affected areas, particularly the armpits, neck, elbow creases, groin, genitals, and perineum (Pita and Vidal-Asensi, 2010). Sulfur mustards are quickly absorbed by the skin after which they initiate an oxidative cascade resulting in an increase of reactive oxygen species (ROS) that lead to the damage of proteins, lipids, and DNA and depletion of the non-enzymatic and enzymatic antioxidant defense systems of the skin. Exposure to sulfur mustards leads to erythema initially that is followed by the formation of blisters, which tend to get infected and necrotized due to the high amount of exudate (Kehe and Szinicz, 2005). Due to the alkylation of the DNA, skin re-epithelization is very slow. The current treatment of blisters caused by CWAs is mainly symptomatic and supportive (Rice, 2003). Melatonin may play a pivotal role in the management of cutaneous lesions induced by these chemical agents, yet its efficacy is dependent on the ability to deliver higher concentrations topically in a targeted manner (Pita et al., 2013).

Melatonin can be crucial in managing skin lesions as it is metabolized to cyclic 3-hydroxy melatonin, N1-acetyl-N2-formyl-5-methoxykynuramine, and N1-acetyl-5-methoxykynuramine (AMK), and all metabolites are highly effective in scavenging free radicals generated by sulfur mustards on the skin (Reiter et al., 2014). Additionally, melatonin can reduce oxidative stress by modulating the nuclear erythroid 2-related factor involved in regulating the antioxidant and cellular protective genes, such as preserving glutathione's integrity (Kleszczynski et al., 2016). This indoleamine can also reduce the inflammatory response and DNA damage due to its capability to inhibit the proinflammatory transcription factor NF-kB and NLRP3 pathways (Ashrafizadeh et al., 2021; Bora et al., 2019). Additionally, melatonin possesses antimicrobial properties, preventing bacterial skin infections (Tekbas et al., 2008a). The mechanism for this antibacterial efficacy is related to the reduction of crucial metabolic substrates necessary for bacterial proliferation. However, this efficacy is more pronounced against gram (−) bacteria in contrast to gram (+) strains (Gancitano and Reiter, 2022; Tekbas et al., 2008b).

The hypothesis underpinning this work is that topically applied melatonin will counteract the oxidative damage and alkylation of cellular macromolecules and enhance cutaneous regeneration. However, significantly greater doses than those utilized for cosmetic purposes, such as anti-ageing (0.1 %), are required to minimize the adverse effects after exposure to CWAs (Milani and Sparavigna, 2018; Milano and Puviano, 2018). Due to the physicochemical properties of melatonin, protection against its chemical degradation and enhancement of its skin permeability is pivotal to the success of such a strategy. Hence, here, we aim to develop self-nano-emulsifying drug delivery systems (SNEDDS) loaded with high melatonin amounts (5 %, 50 mg/g) prepared from generally regarded as safe (GRAS) excipients avoiding the use of irritant solvents and permeation enhancers such as ethanol or diethylene glycol monoethyl ether (Transcutol P). Previous reports have solubilized melatonin in high concentrations (104.6 mg/mL) combining lipids with ethanol (Oh et al., 2001). However, to minimize irritation on the skin, only biocompatible, non-irritant materials were selected. In a recent study, resveratrol and melatonin were formulated as self-nanoemulsifying drug delivery systems (SNEDDS) for ocular administration (Zingale et al., 2024). This study demonstrated the effectiveness of SNEDDS in enhancing the bioavailability of melatonin (Zingale et al., 2024).

SNEDDS offer numerous advantages, including enhanced solubility, improved bioavailability, thermodynamic stability, and reduced oral and topical inter-individual variability (Date et al., 2010), making them an ideal option for enhancing the delivery of poorly soluble drugs like melatonin (Bezerra-Souza et al., 2019; Bezerra-Souza et al., 2021; Lalatsa et al., 2020c). As SNEDDS are isotropic mixtures of oils and surfactants, melatonin will not be in contact with water during storage, as in other lipid-based formulations, to prevent melatonin from oxidizing (Montenegro, 2017). When formulating SNEDDS, 16–48 h of stirring is usually employed to allow the system to reach solubility equilibrium. However, solubility equilibrium can be reached earlier with intense mixing, allowing SNEDDS to be prepared at the point of care prior to administration with microfluidic micromixers and infusion pumps. Microfluidic manufacture based on micromixers is emerging as a continuous, scalable process method for nanomedicines in the post-COVID era, allowing for tight control of their key quality attributes such as size, zeta potential, and drug loading minimizing the need for extensive quality control of numerous batches. Micromixer geometries (channel size and geometry) can be tailored to the product, and 3D printing allows for the facile production of these micromixers (Kara et al., 2021). Nevertheless, the use of 3D-printed micromixers in the fabrication of SNEDDS to reduce the process time to reach solubility equilibrium has not been demonstrated.

A range of generally regarded as safe (GRAS) excipients were evaluated to ensure high solubility of melatonin that guided the choice of excipients for SNEDDS optimization using a D-optimal design of experiments (DOE) targeting high drug loading (50 mg/g) and nanodroplet size (100 nm) upon reconstitution in aqueous media. Melatonin topical permeability, physicochemical characteristics, and antioxidant capacity were further evaluated and compared to other topical melatonin creams. Melatonin-loaded SNEDDS manufactured using conventional mixing methods were compared to those microfluidically manufactured employing 3D-printed micromixers.

2. Materials and methods

2.1. Materials

Melatonin (Ph. Eur. Grade) was purchased from Fagrón Ibérica SAU (Madrid, Spain). SNEDDS excipients, Capryol® 90 (propylene glycol monocaprylate), Labrafil® M 1944 CS (oleoyl polyoxyl-6 glycerides), Labrasol® (caprylocaproyl polyoxyl-8 glycerides), Labrafac® PG (propylene glycol dicaprylocaprate) and Labrafac® lipophile WL 1349 (consisting of medium-chain triglycerides of caprylic (C_8) and capric (C_{10}) acids) were donated by Gattefossé (Saint-Priest Cedex, France). Propylene Glycol, Tween® 80, and Lanette® N wax were purchased from Fisher Scientific (Madrid, Spain). Formvar/Carbon coated Grids-Copper 200 mesh were purchased from Polysciences Europe GmbH (Bergstrasse, Germany). All other chemicals were of ACS reagent grade or above (Sigma Aldrich, Madrid, Spain), and solvents were of HPLC grade (Fisher, Madrid, Spain) and were used as supplied.

2.2. Methods

2.2.1. Melatonin-based cream

Melatonin and excipient amounts are listed in Table 1. A stock solution of preservatives was prepared by dissolving 16 g of methylparaben and 4 g of propylparaben in 96° ethanol (100 mL), and a 1 mL of this ethanol mixture was used in the final melatonin creams. The aqueous phase of the formulation was prepared by combining melatonin, propylene glycol, Tween® 80, and ethanol with the preservatives stock solution volume required and a small quantity of water. This

Table 1
Batch manufacture record (BMR) for melatonin-based cream (5 %, 50 mg/g).

Components	% (w/w)	Provider	Batch
Melatonin	5	Kirsch Pharma	XPSM211023
Propylene glycol	15	Sigma Aldrich	SHBN7271
Tween® 80	5	Sigma Aldrich	BCCF6010
Ethanol 96°	1	Panreac AppliChem	0001898632
Methylparaben (E-218)	0.16	Acofarma	210312-I-1
Propylparaben (E-216)	0.04	Fagrón	L20100042_OF-243915
Sodium metabisulfite (E-223)	0.32	Panreac AppliChem	0001989192
pH adjuster (NaOH)	q.s.to pH 4.5 ± 0.5	Panreac AppliChem	0001892402
Cera Lanette® N	20	Acofarma	181042
Deionized water(Milli-Q 18.2 MΩ·cm)	to 100	Elix 3, Merck Millipore	

Key; q.s.: Quantity sufficient.

mixture was stirred and heated to 60 °C on a heating block to allow for partial solubilization of melatonin.

The remaining quantity of purified water was added, and sodium metabisulfite was incorporated, when the mixture was homogenous. Constant magnetic stirring was maintained to prevent melatonin sedimentation. The pH of the mixture was measured and adjusted to pH 5 using 5 mL of 0.01 M NaOH. Concurrently, the oily phase of the formulation was prepared by melting Lanette® N wax at 65 °C. When the aqueous phase was heated to the same temperature as the oily phase, it was poured into an oily phase under magnetic stirring and brought down to room temperature while mixing till a shiny, thickened emulsion was prepared.

2.2.2. Melatonin solubility studies

Solubility studies in oils, surfactants, and co-surfactants were performed as previously described (Bezerra-Souza et al., 2019). An excess quantity of melatonin, 100 mg, was added to each excipient comprising the SNEDDS. The mixtures were vortexed for one minute and left overnight in a water bath at 37 °C in triplicate. The mixtures were centrifuged at 10,000 rpm for 5 min, and the supernatant (0.01 mL) was diluted with 10 mL of methanol. The absorbance was measured in a spectrophotometer (JASCO V-730 spectrophotometer Madrid, Spain) at 278 nm to determine the solubility of melatonin. A blank SNEDDS with the same dilution in methanol was used as a baseline for background subtraction. A calibration curve was performed previously in methanol to establish the linearity between concentration and absorbance at 278 nm.

2.2.3. Ternary phase diagrams

Ternary phase diagrams were utilized in this study to evaluate the phase behavior of different formulations consisting of three components: Labrasol®, Capryol® 90, and Labrafac® Lipophile WL 1349, with melatonin (50 mg) solubilized in Labrasol®. A D-Optimal design was developed using different mixtures of Labrasol®, Capryol® 90, and Labrafac® Lipophile WL 1349 calculated in the Design Expert 12 software (State Ease, Minneapolis, MN, USA). The following ratio constraints were set before applying quality by design: Labrasol® between 40 to 60 %, Capryol® 90 between 20 and 50 %, and Labrafac® Lipophile WL1349 between 10 and 30 %. These excipients were selected based on the solubility studies above. The sixteen mixtures (Table 2) were vortexed for 5 min, magnetically stirred overnight with a 3 x 5 mm stirring bar at 300 rpm and left at 37 °C using a Fisherbrand™ magnetic hot plate to obtain a homogeneous isotropic mixture in a water bath. The drug solubilized in the SNEDDS was calculated upon centrifugation and dilution in methanol (1:10,000 v/v) by spectrophotometry. Blank SNEDDS were prepared with the same optimal composition except for melatonin dissolved in methanol, which was used to remove any absorbance originating from the blank formulation. The particle size distribution (PSD) was measured (n = 3) after dilution in deionized water (1:1,000 v/v) using a Microtrac Zetatrac (Microtrac, Montgomeryville, PA, USA) with an internal probe ranging from 0.0008 to 6.5 μm. Upon dilution, the optimal excipient combination target for particle size was set at 100 nm, the highest drug loading was selected, and further experiments were performed. Mathematical modeling was performed using multiple linear regression analysis.

2.2.4. Optimization of SNEDDS using quality by design (QbD)

Numerical optimization was undertaken based on the desirability function in terms of size and drug loading. Based on the solubility and phase diagram studies, Labrasol®, Capryol® 90, and Labrafac® Lipophile WL 1349 were selected as the high-hydrophilic-lipophilic balance (HLB 12) surfactant, a medium-HLB surfactant (HLB 5), and the oil (HLB 1) respectively. Optimised SNEDDS was prepared by combining the three as Labrasol®: Capryol® 90: Labrafac® Lipophile WL 1349 (49:33:18 w/w). Melatonin (50 mg/g) was vortexed for 5 min, magnetically stirred overnight with a 3 x 5 mm stirring bar at 300 rpm and left at 37 °C using a Fisherbrand™ magnetic hot plate to obtain a homogeneous isotropic mixture in a water bath. The validation of the optimum formulation was evaluated by comparing the predicted responses with the experimental ones.

Table 2
DoE matrix for optimization of melatonin-loaded SNEDDS.

	Component 1	Component 2	Component 3	Response 1	Response 2	
Run	Labrasol	Capryol 90	Labrafac Lipophile WL1349	Particle size (nm)	MelatoninCorrected Absorbance	MelatoninConcentration (mg/g)
1	0.6	0.26	0.14	107 ± 12	0.239 ± 0.002	48.55
2	0.49	0.33	0.18	120 ± 9	0.212 ± 0.002	43.09
3	0.49	0.21	0.3	122 ± 7	0.240 ± 0.003	48.82
4	0.4	0.34	0.26	70 ± 4	0.237 ± 0.002	48.07
5	0.57	0.33	0.1	108 ± 16	0.250 ± 0.001	50.80
6	0.6	0.2	0.2	108 ± 7	0.178 ± 0.001	36.24
7	0.46	0.28	0.26	137 ± 15	0.258 ± 0.002	52.41
8	0.53	0.26	0.21	157 ± 18	0.176 ± 0.001	35.80
9	0.49	0.21	0.3	76 ± 10	0.224 ± 0.002	45.54
10	0.4	0.34	0.26	34 ± 6	0.233 ± 0.002	47.27
11	0.49	0.34	0.18	77 ± 6	0.249 ± 0.002	50.60
12	0.49	0.34	0.18	94 ± 8	0.226 ± 0.001	45.84
13	0.4	0.42	0.18	129 ± 18	0.208 ± 0.001	42.27
14	0.57	0.33	0.1	51 ± 7	0.223 ± 0.002	45.30
15	0.48	0.42	0.1	62 ± 8	0.215 ± 0.001	43.65
16	0.4	0.5	0.1	65 ± 8	0.183 ± 0.002	37.33

Note: Excipient quantities are expressed as fractions, with the total sum of all excipients equaling 1 g. The average particle size (n = 3) was measured after dilution in deionized water (1:1,000 v/v), and the average absorbance (n = 3) was illustrated for each combination

2.2.5. In-vitro Franz cell permeability studies

Diffusion studies of optimized melatonin-loaded SNEDDS (50 mg/g) were performed using vertical diffusion Franz cells (Soham Scientific, Loughborough, UK) as previously described (Fernandez-Garcia et al., 2020; Serrano et al., 2019). The effective diffusion area was 1.76 cm^2 with a cell volume of 12 mL. Strat-M® membranes (Merck KGaA, Darmstadt, Germany) were placed on the receptor compartment directly as they are synthetic models for transdermal diffusion testing (Strat-M® Membrane for Transdermal Diffusion Testing, 2023). A stirring bar (3 x 5 mm) was added to each Franz cell's receptor compartment filled with PBS (pH 7.4). Optimized melatonin-loaded SNEDDS was added to the donor chamber (0.5 g). At selected time points (0, 15, 30, 60, 90, 120, 240, and 360 min), 1 mL of the receptor medium was taken and immediately refilled with 1 mL of fresh media. Melatonin concentration was quantified using the USP38 HPLC method described below (Jasco Inc., Maryland, USA)(Monograph, 2023). The melatonin cream described above was used for comparison purposes, and permeability was tested under the same conditions.

The cumulative amounts of melatonin permeated through the Strat-M® membrane were plotted as a function of time (Serrano et al., 2019). Regression analysis was used to calculate the slopes and intercepts of the linear portion of each graph. The following equation (Eq. (1) was applied to calculate the steady-state flux:

$$Jss = \frac{dC}{dt} * \frac{1}{A} \quad (1)$$

where *Jss* is the steady-state flux (μg/cm^2/h), dC/dt is the amount of melatonin permeating the membrane over time (μg/h), and A is the surface area of contact of the formulation (cm^2) (Lalatsa et al., 2016). The permeability coefficient (P) was calculated by using Equation (2):

$$P = \frac{Jss}{cd} \quad (2)$$

where cd is the amount of drug applied in the donor compartment (0.5 g of formulation equivalent to 25 mg of melatonin). The diffusion coefficient was calculated by using the following equation:

$$D = Ph \quad (3)$$

where h is the thickness of the membrane (0.25 cm) (Kaur et al., 2018).

2.2.6. Quantification of melatonin by HPLC

Melatonin was quantified using a validated HPLC method described in the USP 38 food supplements (Melatonin USP Monograph, 2023); A Jasco HPLC, which was equipped with a Jasco PU-1580 pump, a Jasco AS-2050 Plus autosampler, and a Jasco UV-1575 UV–visible detector to a Waters Spherisorb® S10 ODS1, C18, (4.6 x 200 mm, 5 μm) was used. Integration of the peaks was performed with the program Borwin 1.5 for PC (JMBS Developments). The mobile phase consisted of 75:25 v/v phosphate buffer: acetonitrile HPLC grade. Phosphate buffer was prepared by dissolving 0.5 g of monopotassium phosphate in 1 L of purified water and addition of 1:10 v/v diluted orthophosphoric acid to adjust the pH to 3.5. The mobile phase was filtered by a 0.45 μm hydrophilic filter (Supor®-450, Pall Corporation Ref 60173, Port Washington, NY, USA). The isocratic flow rate was 1.5 mL/min. The injection volume was set at 10 μL and the wavelength at 222 nm. The retention time for melatonin was 3.7 min.

2.2.7. Physicochemical characterization

Stability studies.

Freshly prepared melatonin-loaded SNEDDS was stored in HPLC vials at 25 °C and protected from moisture by sealing the container with parafilm and from light by covering it in aluminum foil. Stability samples were taken in triplicate at different time points (Day 0, 30, 180, and 360). The melatonin content in these samples was quantified by a previously validated HPLC method.

Rheological profile evaluation

The melatonin-loaded SNEDDS and the melatonin cream were equilibrated to 25 °C. The measurements were performed in triplicate using an AR2000 Rheometer (TA Instruments, Elstree, UK) equipped with a 4 cm flat plate geometry. The rheology was tested according to the evolution of shear stress versus shear rate. The rheometer was configured to linearly increase the shear rate by 0.33 Pa/s up to 215 s^{-1} for melatonin-loaded SNEDDS and deionized water, and up to 95 s^{-1} for the melatonin cream. The collected data was analyzed using TA Universal Analysis software.

Near-infrared (NIR) Spectroscopic analysis.

The VIAVI MicroNIR 1700 (Onsite W, Viavi, MTBrandao, España) spectrometer was used for near-infrared (NIR) spectroscopic analysis. The instrument was calibrated strictly following the manufacturer's instructions, which included establishing an accurate baseline and negating any potential noise specific to the instrument using its built-in reference system. Spectra were collected with interleaved scans in the 900–1660 nm range. Measurements of optimized SNEDDS formulation containing melatonin and the individual components (unprocessed melatonin, Capryol 90, Labrafac Lipophile WL 1349, and Labrasol) were performed in triplicate for each sample. Multivariate data analysis was conducted utilizing Unscrambler® X software (CAMO Software, Oslo, Norway). The pre-processing transformation involved data normalization followed by second derivative Savitzky-Golay smoothing (7 points) as previously described (Rodriguez Fernandez et al., 2022).

2.2.8. Hydroxyl radical scavenging activity of melatonin-loaded SNEDDS

The hydroxyl radical scavenging assay was conducted to assess the antioxidative properties (Chobot, 2010). Melatonin-loaded SNEDDS were dispersed in a KH_2PO_4/KOH buffer (30 mM, pH 7.4) to achieve melatonin concentrations ranging from 10 to 5000 μg/mL. For each assay, melatonin formulations were mixed with a 10.4 mM 2-deoxy-D-ribose solution (5:1, v:v, 300 μL total volume), followed by the addition of a 50 μM ferric chloride (100 μL $FeCl_3$) solution prepared in the same buffer. Two series of experiments were prepared depending on the presence or absence of EDTA in the media. In the EDTA studies, the $FeCl_3$ solution contained 52 μM EDTA, premixed in a 1:1 vol ratio, while in the no EDTA studies, the EDTA was replaced with an equivalent buffer volume, allowing direct iron chelation by melatonin.

Reactions in both series were initiated by adding 10 mM hydrogen peroxide (50 μL) solution and 1.0 mM ascorbic acid solution (50 μL) (Chobot, 2010; Chobot and Hadacek, 2011). After vortexing, the mixtures were incubated at 37 °C for one hour. The reactions were terminated by adding butylated hydroxytoluene (BHT, 20 μL) and 1.0 % thiobarbituric acid (TBA) solution in 3 % trichloroacetic acid (250 μL). After vortexing, the samples were heated at 85 °C for 20 min in a water bath and then immediately transferred to an ice bath for 5 min to stop the reaction. The resulting malondialdehyde-thiobarbituric acid (MDA-TBA) adducts were extracted with n-butanol (700 μL), and the absorbance of an aliquot of the n-butanol layer was measured at 532 nm using a microplate reader (SpectraSTAR Nano BMG Labtech, Madrid, Spain). Each assay was conducted in triplicate. Positive control was included for both series (with and without EDTA), containing all reaction components except the melatonin-loaded SNEDDS, corresponding to a 100 % MDA formation baseline. A negative control, consisting of the complete reaction mixture without 2-deoxy-D-ribose, was used to account for any background interference. Antioxidant activity was calculated based on the percentage of scavenging relative to control samples to determine the 50 % scavenging concentration (SC_{50}) from the dose–response curve (Dorman et al., 2004). The following equation (Eq. (4) was applied:

$$\text{Scavenging Percentage}\,(\%) = \frac{AbsControl - AbsSample}{AbsControl - AbsBlank} \quad (4)$$

2.2.9. Microfluidic manufacture of SNEDDS using 3D-printed chips

Manufacture of 3D printed micromixers using

stereolithography (SLA).

A T-shaped toroidal micromixer microfluidic chip was designed using Solidworks® (Autodesk®, Mill Valley, CA, USA) with 7.8 cm in length, 5.6 cm in width, and 0.6 cm in height. The microfluidic chip consisted of two distinct inlet channels measuring 2 cm in length and 1 mm in diameter up to the junction of the inlets with six interlinked circular channels measuring 0.5 cm in diameter and 0.1 mm in channel diameter through the outlet channel. The 2-inlet, six interlinked circular channels, and a 1-outlet microfluidic chip design was exported into a standard tessellation language (.stl) digital file. This file was imported into Anycubic Photon Slicer Software (Anycubic®, Shenzhen, China). The (.stl) file was sliced to g-code format (.pwmx) for SLA printing.

The Anycubic® Photon Mono X SLA printer was used to print microfluidic chips under photopolymerization of the Anycubic® UV sensitive resin (transparent) at 405 nm. The solidified resin was adhered initially to the metal platform, and the other layers adhered to this first layer, thus creating the desired object. Each layer was 0.05 mm thick. The first eight layers were exposed to UV light longer than the others (60 s) to ensure good attachment to the metallic platform. The remaining layers were exposed to UV light for 2 s. At the end of each layer, the UV light was turned off for 1 s, preventing unwanted parts from solidifying. The total number of layers required to form the microfluidic chip using the SLA printer was 1633.

Another T-shaped toroidal micromixer was also 3D printed using Fused Deposition Modeling (FDM), as previously reported for comparison purposes (Tiboni et al., 2021). To produce the microfluidic chips, polypropylene (PP, BASF, Germany) was used in a FDM 3D printer (Ultimaker 3, Ultimaker, The Netherlands) with a print speed of 25 mm/s and a nozzle temperature of 225 °C (0.25 mm nozzle). A PP (Polypropylene) adhesion sheet (Ultimaker, Netherlands) was applied to the build plate, and its temperature was set at 85 °C. The design was printed with a 100 μm layer height and a 100 % infill density.

2.2.10. Numerical simulations

Based on Reynolds number (*Re*), the impingement process of two inlet streams can be classified into two different laminar flow regimes in the mixing channel: stratified flow ($0 < Re \langle 50$), vortex flow ($50 < Re \langle 150$), and engulfment 245 flow ($150 < Re \langle 300$). The Reynolds Number in the mixing central channel (Re) was calculated according to equation (5):

$$\mathrm{ReM} = \frac{\rho_{mix} \cdot v \cdot L}{\mu_{mix}} \tag{5}$$

where ρ_{mix} is the density of the mixture, v is the velocity in the mixing channel, L is the characteristic length of the channel that for a circular cross-section is equal to the inner diameter (D), and μ_{mix} is the dynamic viscosity of the mixture.

The fluid velocity in the channel (v) was calculated according to Eq. (6):

$$v = \frac{Q}{A} \tag{6}$$

where Q was the volumetric flow rate calculated as the sum of the volume flow rate of Labrasol and Capryol 90 + Labrafac Lipophile WL1349 mixture, and A was the channel cross-section area calculated according to Eq. (7):

$$A = \frac{\pi D^2}{4} \tag{7}$$

where D is the inner diameter of the channel.

The volumetric ratio for Labrasol and Capryol 90 + Labrafac Lipophile WL1349 (CapLab) mixture was used to calculate the mixture's density and viscosity following Eq. (8) and (9):

$$\rho_{mix} = \frac{V_{Labrasol} \cdot \rho_{\mathrm{CapLab}} + V_{Labrasol} \cdot \rho_{Labrasol}}{V_{\mathrm{CapLab}} + V_{Labrasol}} \tag{8}$$

$$\mu_{mix} = \frac{V_{\mathrm{CapLab}} \cdot \mu_{\mathrm{CapLab}} + V_{Labrasol} \cdot \mu_{Labrasol}}{V_{\mathrm{CapLab}} + V_{Labrasol}} \tag{9}$$

where the density of the Labrasol ($\rho_{Labrasol}$) was1059 $\frac{kg}{m^3}$; the density of the Capryol 90 + Labrafac Lipophile WL1349 mixture (ρ_{CapLab}) was 965.2 $\frac{kg}{m}$ ^{3}; the viscosity of Labrasol (μ_{Labrasol}) was 0.08 $Pa\hat{A}{\cdot}s$ and the viscosity of Capryol 90 + Labrafac Lipophile WL1349 mixture (μ_{CapLab}) was 0.0212 $Pa\hat{A}{\cdot}s$ (Technology). V was the volume utilized for each phase.

Computational fluid dynamics (CFD) simulations were performed using COMSOL Multiphysics 5.6 (Burlington, MA, USA), incorporating laminar flow and diluted species interface transport. A T-shape toroidal micromixer model was employed to align the simulation with the experimental setup. Flow rates for each inlet and fluid property were determined based on the design of the experiment approach and formulation specifics.

Momentum and mass conservation were analyzed in the microfluidic chips, characterized by single-phase, incompressible, and time-dependent laminar flow. This analysis was conducted using the Navier-Stokes equations for momentum (Eq.10) and the continuity equation (Eq.11) for mass conservation. The equations are expressed as follows:

$$\rho\left(\frac{\partial \boldsymbol{u}}{\partial t} + \boldsymbol{u}\cdot\nabla\boldsymbol{u}\right) = -\nabla p + \mu\nabla^2\boldsymbol{u} \tag{10}$$

where (ρ) is the fluid density (kg/m^3), (u) is the fluid velocity vector (m/s), (t) is time (s), (p) is pressure (Pa), and (μ) is the dynamic viscosity (Pa.s).

$$\rho\nabla\cdot\boldsymbol{u} = 0 \tag{11}$$

The equation implies that the fluid is incompressible. The resolution of these equations yielded valuable insights into the velocity and pressure distributions within the system. Subsequently, the resulting velocity distribution was employed to ascertain the concentration field of species, computed via the convection–diffusion equation, formulated as:

$$\frac{\partial c_i}{\partial t} + \nabla\cdot(-D_i\nabla c_i + \boldsymbol{u}c_i) = R \tag{12}$$

where (c_i) is the concentration of species (i), (D_i) is the diffusion coefficient (estimated value for mixture of Labrasol and CapLab was 7 .28x 10^{-12} m^2/s (Fanun, 2007)), and ($\boldsymbol{u}$) is the fluid velocity vector. R is the reaction rate, which was assumed to be zero. The concentration of species considered 1 mol/m^3 for both phases.

Prior investigations (Chen and Shen, 2017; Javaid et al., 2018; Ta et al., 2015) have employed techniques reliant on concentration standard deviation to evaluate mixing within microfluidic chips. In this research, the efficiency (M) was determined utilizing a formula derived from concentration standard deviation, expressed as follows:

$$M = 1 - \frac{\sigma}{\sigma_{Max}} \tag{13}$$

where (σ) represents the standard deviation of species concentration at a given cross-section, while (σ_{Max}) indicates the standard deviation in a completely unmixed state. The efficacy, indicated as 'M', is quantified on a scale where 0 corresponds to the unmixed state and 1 to a fully mixed state. The standard deviation for this purpose is calculated as follows:

$$\sigma = \sqrt{\frac{1}{N}\sum_{i=1}^{N}(c_i - c_m)^2} \tag{14}$$

where (N) is the number of sampling points, (c_i) is the mixing fraction at point (i), (c_m) is the optimal mixing fraction.

2.2.11. Continuous microfluidic manufacture of melatonin-SNEDDS with SLA and FDM 3D printed chips

Taking into account the optimized ratio obtained from the QbD studies, melatonin (500 mg) was initially dispersed in Labrasol® with magnetic stirring at 300 rpm at 37 °C for 15 min (4.9 g). Capryol® 90 (3.3 g) and Labrafac® Lipophile WL1349 (1.8 g) were combined dropwise under magnetic stirring at 300 rpm and a temperature of 37 °C. Phase uniformity was ensured by combining the ingredients dropwise with constant magnetic stirring at 300 rpm, maintaining a temperature of 37 °C, and a visual inspection. Large quantities of both phases (100 g) were prepared in advance. The phases were loaded into 10 mL syringes attached to syringe pumps (New Era Pump Systems, Farmingdale, NY, USA). Syringes were fitted with a 14-gauge olive-colored needle (OD 1.83 mm) (Fisher Scientific, Madrid, Spain). Silicone tubes (ID of 1.83 mm) (Fisher Scientific, Madrid, Spain) were connected between the syringe needle outlet and the micromixer inlet.

The flow rates of both phases were set to 0.5 mL/min to achieve a 1:1 v/v ratio. Micromixers were first eluted with blank SNEDDS for 5 min at the same flow rate and ratio to remove any impurities potentially within the micromixer channels. The eluate melatonin-SNEDDS (10 g) was collected. The process was repeated in triplicate using the SLA and the FDM micromixers. Particle size, polydispersity, and morphological appearance were evaluated.

2.2.12. Characterization of melatonin-SNEDDS formulations

Freshly prepared formulations were diluted 1:1,000 v/v with deionized water (pH 6.5) before further characterization by TEM and particle size.

Morphological evaluation.

A drop of the formulations, melatonin-loaded SNEDDS, SLA-printed microfluidic SNEDDS, and FDM-printed microfluidic SNEDDS was diluted in deionized water (1:1,000 v/v) and placed onto a 3.05 mm diameter copper 200 mesh Formvar/Carbon-coated grid, prior staining with 2 % uranyl acetate and the excess sample was blotted off with Whatman No. 1 filter paper. TEM was performed using a JEOL 1400 transmission electron microscope (JEOL Ltd., Tokyo, Japan) operating at 120 KV. An AMT digital camera was used to capture the images.

Particle size distribution.

The particle size distribution (PSD) was measured in triplicate (n = 3) using a Microtrac Zetatrac (Microtrac, Montgomeryville, PA, USA) with an internal probe ranging from 0.0008 to 6.5 μm. The polydispersity index (PDI) and the span were calculated.

$$Span = \frac{D90 - D10}{D50} \tag{15}$$

$$Polydispersity\ Index = \frac{\sigma}{\mu} \tag{16}$$

where σ is the standard deviation, and μ is the mean particle diameter.

3. Results

3.1. Solubilization studies

Melatonin solubility was evaluated in different excipients (Fig. 1) and was higher in Labrasol® with an HLB of 12 (123.17 ± 1.47 mg/g, HLB:12), while 3-fold lower solubility was measured in the co-surfactants, Capryol® 90 (HLB 5) and Labrafil® M 1944 CS (HLB 9). The solubility of melatonin in oily vehicles was poorer, being significantly greater in Labrafac® lipophile WL 1349 than in Labrafac® PG. Thus, Labrasol®, Capryol® 90, and Labrafac® lipophile WL 1349 were selected as the surfactant, co-surfactant, and oily vehicle for further pseudo-ternary diagrams.

3.2. Optimization of melatonin-SNEDDS formulation

Sixteen runs were performed in the D-optimal mixture design of experiments (Table 2). A different set of constraints were selected based on the solubility profile of melatonin. The different SNEDDS ratios are illustrated in Table 2, as well as the two responses evaluated for each formulation, the particle size expressed in nanometers after 1 in 1,000 (v/v) dilution in water, and the amount of melatonin solubilized expressed as absorbance after a 1 in 10,000 v/v dilution in methanol.

A ternary phase diagram (Fig. 2A&B) was constructed to evaluate the phase behavior of oil and surfactants over the studied concentration range. Particle size expressed in numbers allowed us to develop a better predictive model with a higher R^2 than the size expressed in volume. The

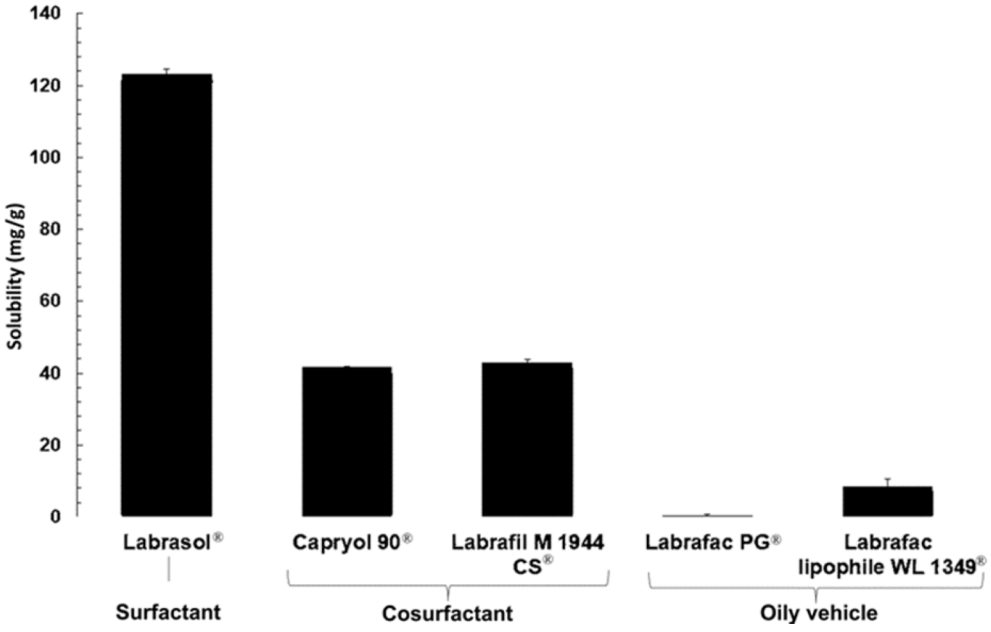

Fig. 1. Solubility of melatonin in different vehicles.

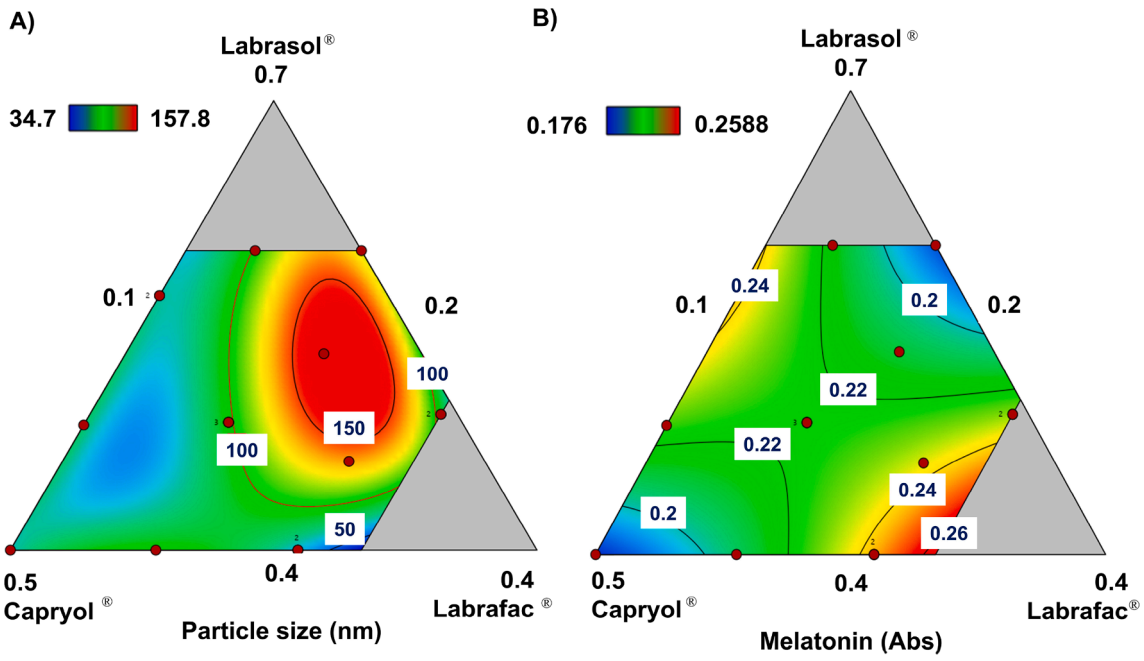

Fig. 2. D-Optimal design of experiment of melatonin-loaded SNEDDS. A) Particle size; **B.** Absorbance as a surrogate for drug loading.

blue region indicates the self-nanoemulsifying region, corresponding with a lower particle size (<100 nm) (Fig. 2A). The particle size significantly increases, when the amount of Capryol® is reduced. This change can be related to the significant difference in HLB between Labrasol® and Labrafac® Lipophile, requiring a co-surfactant to yield reduced particle sizes. Large amounts of oily vehicles also resulted in larger droplet sizes.

The amount of melatonin solubilized in the SNEDDS is illustrated in Fig. 2B. In this case, the surface response model that better fitted the experimental results was quadratic. The optimal region with greater drug loading was localized in two different sections of the ternary phase diagram. The first region was found within the composition with low Labrafac® lipophile quantities, which was expected considering the lower solubility of the drug in this excipient, but the second region of high melatonin loading was located surprisingly in the border of a high Labrafac® ratio, which can be associated with the smaller particle size of the SNEDDS formed after self-emulsification in this area.

Predictive model equations.

The predictive model equations of particle size and melatonin solubility are given below:

$$\begin{aligned} \textit{Particle Size} = {} & 339.047{*}A + 68.0375{*}B + {-}1011.66{*}C \\ & + {-}447.427{*}AB + 2016.91{*}AC + 2226.57{*}BC \\ & + {-}2110.15{*}ABC + {-}16.7148{*}AB(A-B) \\ & + {-}3015.2{*}AC(A-C) + {-}999.772{*}BC(B-C) \end{aligned} \quad (17)$$

$$\begin{aligned} \textit{Melatonin Solubility} = {} & {-}1.60104{*}A + {-}1.71286{*}B + {-}1.03274{*}C \\ & + 0.941189{*}AB + {-}1.23404{*}AC \\ & + {-}0.267892{*}BC \end{aligned} \quad (18)$$

where A, B and C represent the proportions of Labrasol®, Capryol® 90, and Labrafac® Lipophile WL 1349, respectively.

The p-values for the overall model were 0.0366 for particle size and 0.0471 for melatonin solubility, indicating that both models are statistically significant. The R^2 values for the particle size and melatonin solubility models were 0.8757 and 0.6297, respectively, indicating a good fit for the data with adjusted R^2 values of 0.6893 and 0.4446 respectively.

Validation studies were conducted by formulating the suggested optimal SNEDDS mixture, which was designed to target a 100 nm particle size upon dilution and the highest drug loading. The optimized SNEDDS consisted of Labrasol®: Capryol® 90 and Labrafac® Lipophile WL 1349 in a 49:33:18 wt ratio and exhibited a particle size of 102 ± 3 nm upon dilution and a drug loading of 50 mg/g. The predicted particle size and melatonin solubility were 101 nm and 43.6 mg/g, respectively, confirming the model's reliability.

Multivariate statistical methods, including multiple linear regression and analysis of variance (ANOVA), were employed to identify and quantify the relationships between particle size and melatonin solubility. The statistical analysis validated the significance of the predictors and their interactions, thereby providing a reliable model for optimization. The ANOVA results indicated that the model for particle size was significant, with an F-value of 4.70 and a p-value of 0.0366. Similarly, the model for melatonin solubility had an F-value of 3.40 and a p-value of 0.0471. Further permeability and stability studies were performed using the optimized formulation.

3.3. *Permeability studies*

In vitro permeability studies were carried out using synthetic Strat-M® membrane, which is a non-animal-based model for transdermal diffusion testing that is predictive of diffusion in human skin without batch-to-batch variability, safety, and storage limitations, taking into account the physicochemical properties of melatonin (log P: 1.4 and molecular weight: 232 g/mol). Melatonin-loaded SNEDDS showed a 42-fold higher steady-state transdermal flux (169 μg/cm^2/h) (Fig. 3A, & Table 3) compared to the melatonin cream (~4 μg/cm^2/h) (Fig. 3B, & Table 3) as well as a higher flux than other values reported by other authors for melatonin encapsulated within liposomes (10.9 μg/cm^2/h), elastic lipidic vesicles (51 μg/cm^2/h) or just plain drug in aqueous solution (4.2 μg/cm^2/h) (Dubey et al., 2006). The lag time of the optimized formulation was 15 min as in the case of SNEDDS self-emulsification is required (Dubey et al., 2006; Lalatsa et al., 2020a). The optimal performance of the SNEDDS can be attributed to their smaller particle size (≈ 100 nm) but also the high drug gradient concentration achieved.

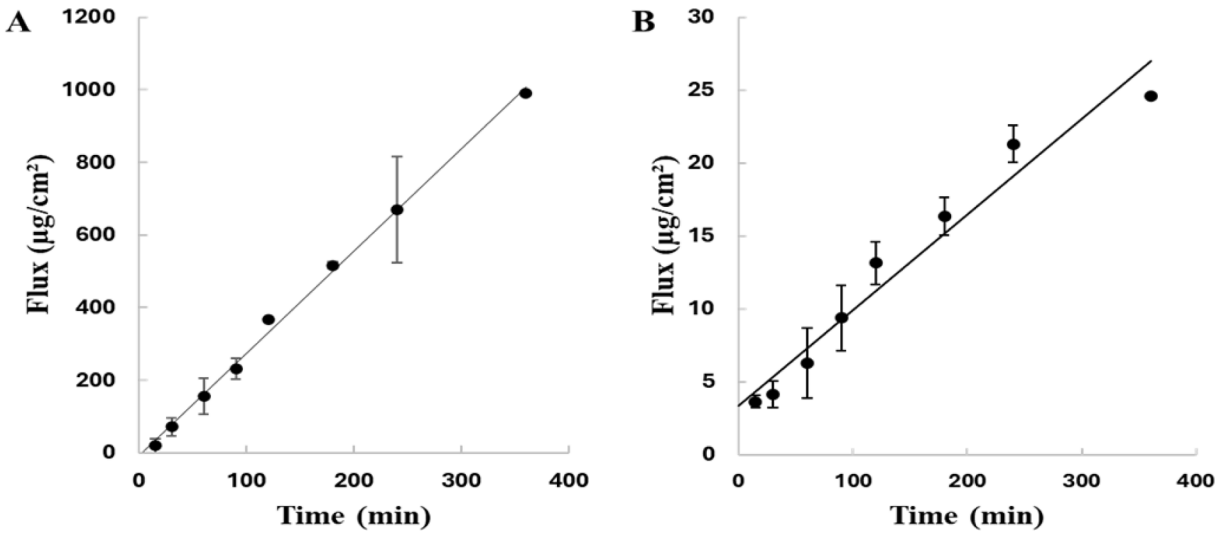

Fig. 3. *In vitro* permeability evaluation across Strat-M® membrane. A) Melatonin-loaded SNEDDS formulation. **B.** Melatonin cream formulation.

Table 3
In vitro permeability parameters of melatonin cream and melatonin-loaded SNEDDS.

Formulations	Jss (µg/cm²/min)	Jss (µg/cm²/h)	T_{lag}(min)	Permeability Coefficient (x10³) (cm/h)	Diffusion Coefficient (x10³) (cm²/h)
Melatonin SNEDDS	2.83 ± 0.40	169.85 ± 24.18	15.22 ± 4.36	6.8 ± 1.0	1.7 ± 0.2
Melatonin Cream	0.0657 ± 0.0034	3.94 ± 0.20	–	0.2 ± 0.01	0.039 ± 0.002

Key: Jss, steady-state transdermal flux calculated from the slope of the Cartesian plot of the cumulative amount of the drug present in the receptor compartment versus time; T_{lag}: Lag time (h); P, permeability coefficient (cm/h) calculated by using the formula Jss/cd (cd is the amount of drug applied in the donor compartment, so 500 mg of formulation which is equivalent to 25 mg of melatonin); D, diffusion coefficient (cm²/h) calculated by using formula Jss = d.k/h × cd (where h is the thickness of the Strat-M®).

3.4. Physicochemical chemical characterization

Stability Studies.

Melatonin-loaded SNEDDS were stable over 12 months when stored at 25 ℃ (drug content > 95 %) (Fig. 4). No visual changes in the color of the formulation were recorded at any time point. These results show excellent stability for long-term use at 25℃ when protected from light and moisture compared to previous stability studies that indicated poor stability in aqueous media (Pranil et al., 2020).

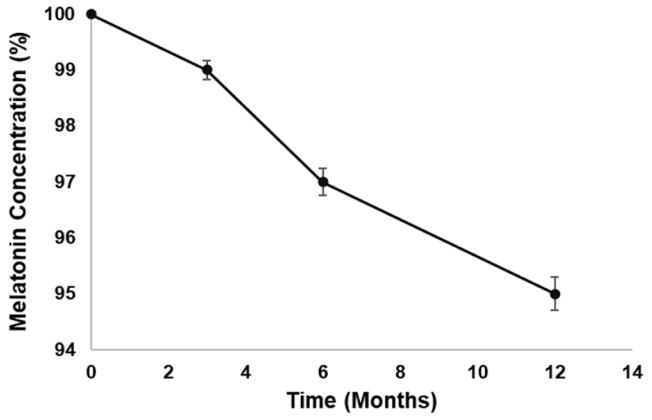

Fig. 4. Chemical stability of melatonin-loaded SNEDDS formulation for 12 months expressed as the average melatonin content (%) ± standard deviation (n = 3).

Rheological profile evaluation.

Melatonin-loaded SNEDDS exhibited non-Newtonian, shear-thinning (pseudoplastic) behavior at lower shear rates (Fig. 5A). The melatonin-loaded SNEDDS exhibited a 10-fold higher viscosity than deionized water which facilitates its application on the skin. Furthermore, a comparative analysis of the rheological properties between the melatonin SNEDDS and the melatonin cream was conducted to ensure the SNEDDS's suitability for patient application. Both formulations exhibited a shear-thinning behavior but the cream's viscosity was significantly higher (Fig. 5B).

NIR analysis.

NIR spectra of all individual components and the melatonin-loaded SNEDDS are presented in Fig. 6. Data normalization and the application of the second derivative to the spectra revealed two distinctive bands for Labrasol, Capryol 90, and Labrafac Lipophile WL1349 at 1625 nm and 1120 nm. The same bands were also present for the melatonin-loaded SNEDDS, although they were notably different from the pure melatonin spectra. The bands at 1625 nm and 1120 nm are indicative of the —CH, —CH_2, and —CH_3 group's first and second overtones, respectively, but also the band at 1120 nm is related to —OH groups. In contrast, the NIR spectra of melatonin SNEDDS exhibited a prominent band at 1480 nm, which is attributed to the first overtone of the —NH group. This band indicates the potential formation of hydrogen bonds between melatonin and the hydroxyl groups of the SNEDDS excipients upon solubilization.

3.5. Hydroxyl radical scavenging activity of melatonin-loaded SNEDDS

The antioxidative capacity of melatonin-loaded SNEDDS was evaluated through their ability to scavenge hydroxyl radicals generated in a Fenton reaction system (Fig. 7) (Gutteridge, 1994). The melatonin-loaded SNEDDS exhibited a concentration-dependent response. In the presence of EDTA, the calculated SC_{50} value, representing the melatonin concentration for a 50 % reduction in the radical presence, was 640.5 ± 50.7 µg/mL. In contrast, in the absence of EDTA, the SC_{50} value was 4-fold reduced to 144.7 ± 18.8 µg/mL p-value < 0.05), indicating an enhanced antioxidant capacity attributable to unimpeded iron chelation by melatonin (Gulcin et al., 2003). However, the antioxidant capacity of melatonin was relatively limited under competitive chelation conditions facilitated by EDTA. While melatonin-loaded SNEDDS demonstrated a

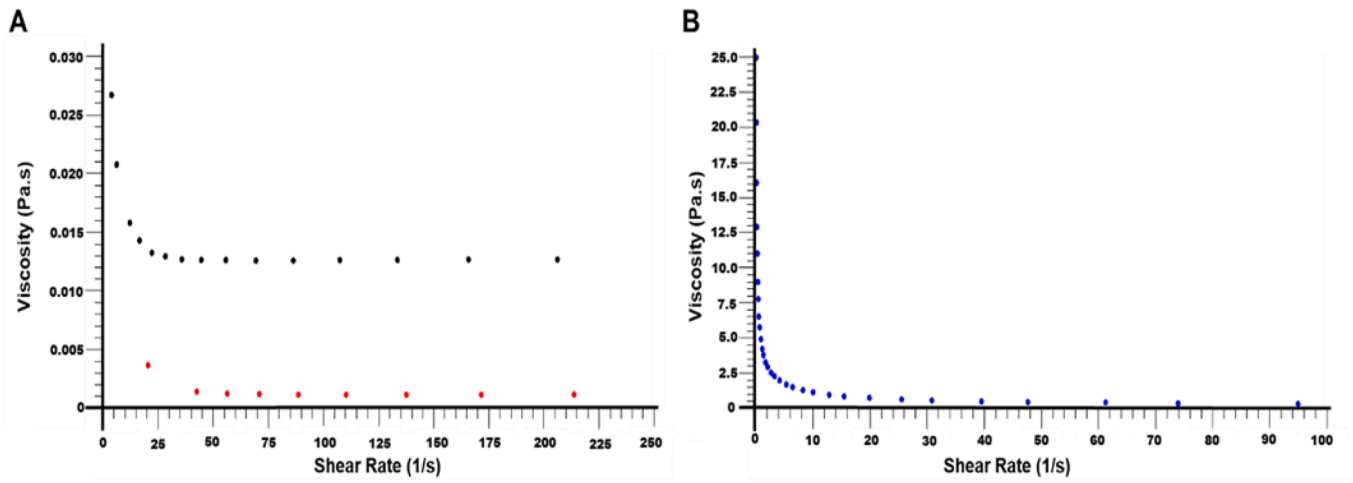

Fig. 5. Rheological behaviors of melatonin formulations. Key: **A.** (—●-) Melatonin-loaded SNEDDS, (—●-) Deionized water, **B.** (—●-) Melatonin cream.

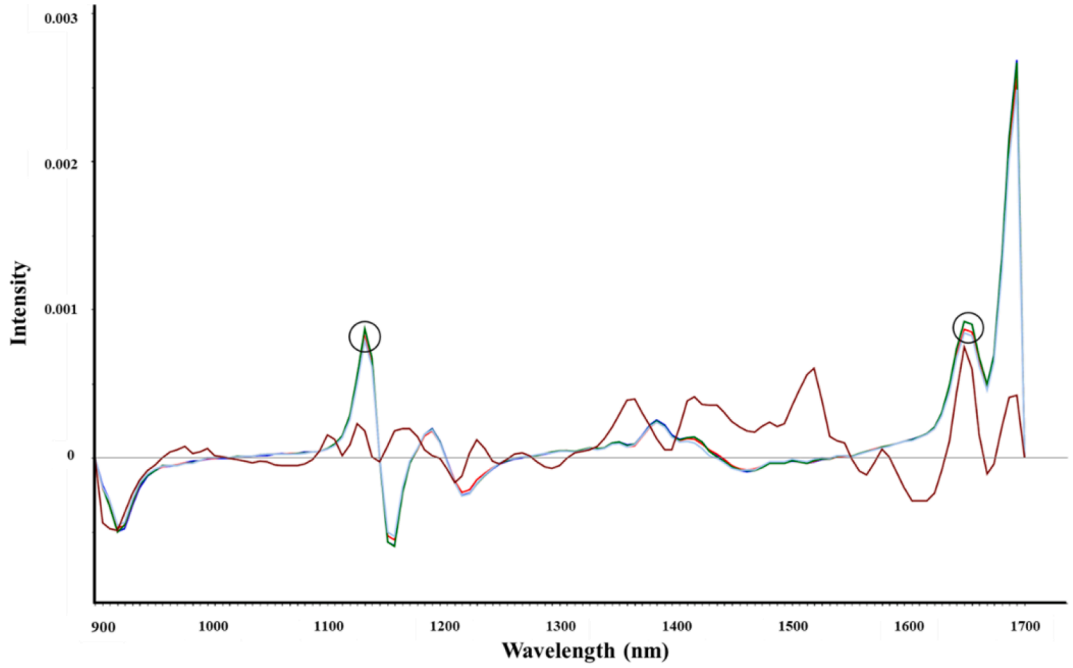

Fig. 6. NIR spectra of melatonin-loaded SNEDDS (blue line) compared to unprocessed melatonin (dark red line), Labrasol (red line), Capryol 90 (green line), Labrafac Lipophile WL1349 (light blue line) after data normalization and Savitzky-Golay second derivative.

concentration-dependent increase in hydroxyl radical scavenging activity at lower concentrations, a decrease in antioxidant capacity was observed as the melatonin concentration increased beyond 40 μg/mL. This trend indicates a complex balance between antioxidant and pro-oxidant activities depending on the melatonin concentration, which is a common phenomenon in redox biology where agents with antioxidant properties can display dual roles depending on the environment and concentration (Zhang and Zhang, 2014).

3.6. Numerical simulations and microfluidic manufacture of melatonin-SNEDDS using 3D-printed chips

In Fig. 8A–C, the computer-aided design (CAD) for the 3D printed chip using SLA technology is illustrated, and the final successful 3D printed prototype is presented along with the dimensions of the internal channels.

Numerical simulations were performed to investigate the mixing efficiency inside this particular geometry and channel size. The Reynolds number (Re) was determined to assess the flow regime within the microchannels of the T-shaped toroidal micromixer. The Re was 0.71, corresponding with a laminar flow, indicating that molecular diffusion is the primary mechanism for mixing the two phases within the micromixer. The velocity field within the T-shaped toroidal microfluidic showed apparent convergence of the flow streams at the junction where the two inlets merge (Fig. 9A). The velocity magnitude in this region showed the highest values, reaching up to 0.08 m/s. The streamlines displayed within the microfluidic channels confirmed the presence of a laminar flow regime.

The concentration gradient within the channels is shown as a progressive increase from the inlet, where mixing between phases has not occurred yet. As the solute advanced through the series of toroidal rings, a gradual transition through the color spectrum was observed, resulting

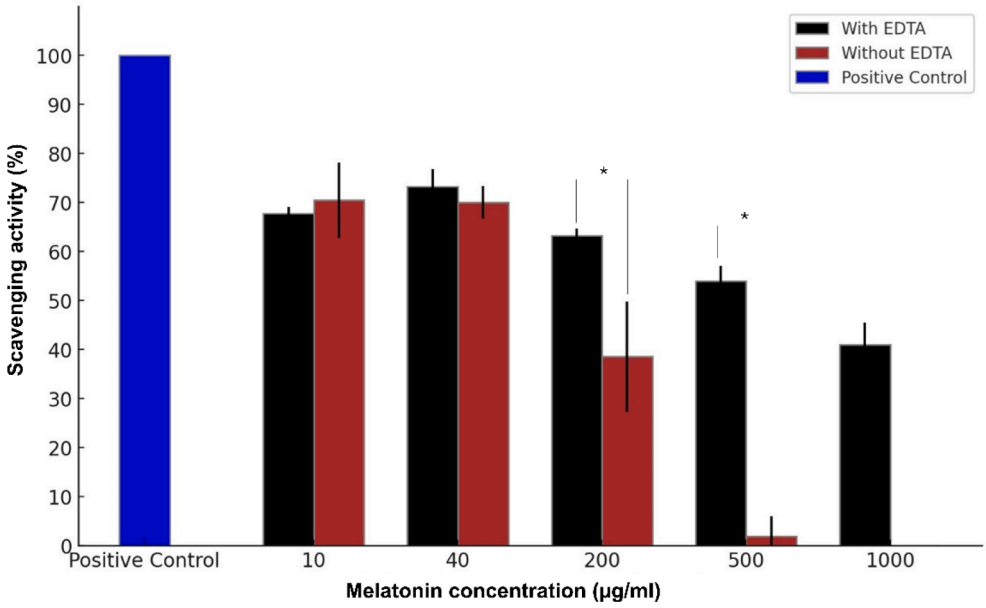

Fig. 7. Comparison of scavenging activity at different melatonin concentrations with and without EDTA. Black bars indicate scavenging activity with EDTA, while red bars indicate scavenging activity without EDTA. The blue bar represents the positive control, indicating 100 % scavenging activity. *Statistically significant differences ($p < 0.01$).

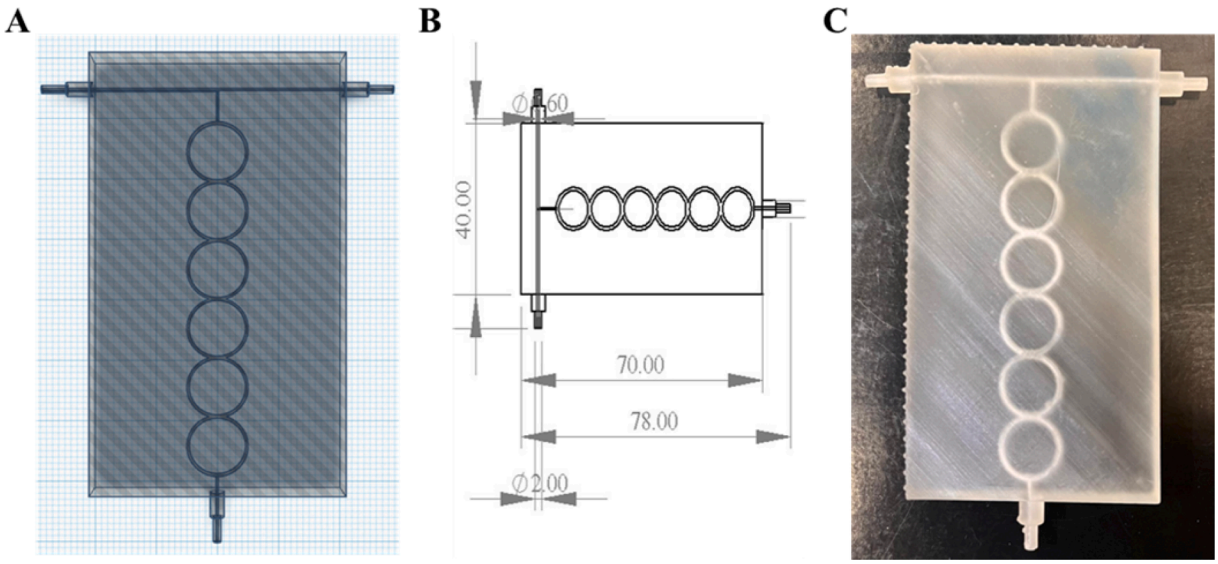

Fig. 8. Design, dimensions, and image of the 3D printed microfluidic chip. Key: **A.** Computer-aided design of T-shaped toroidal micromixer (.stl file); **B.** Geometrical design and dimensions of the 3D printed micromixer obtained from Solidworks 2020 software (mm) **C.** Photograph of the 3D printed microfluidic chip by SLA obtained from an iPhone 13 camera (12 MP).

in a green color that indicates optimal mixing, considering that both phases are flowing in a 1:1 ratio (Fig. 9B).

Color-coded concentration mapping was used to reveal the spatial interaction and phase distribution of the two phases within the microfluidic chip (Fig. 9C).

The heterogeneous mixing within the cross-section of the phases was simulated using COMSOL, as depicted in Fig. 9C. A detection limit for mixing was set at concentrations where any section with two phases present above 1 % to facilitate this analysis. In the visualization, red represents areas where the concentration of two phases is above this detection limit. Conversely, regions colored in green indicate areas where one of the phases is either completely absent or present at concentrations below the 1 % detection limit. This differentiation helps to clearly visualize the distribution and mixing efficiency of the phases within the SNEDDS formulation. The initial concentration for each phase was standardized at 1 mol/m^3. Standardizing the initial concentration at 1 mol/m^3 provides a consistent baseline, ensuring that any observed differences in mixing are due to the process itself rather than variations in starting conditions.

The results of the simulation indicated that the channel length required to achieve complete heterogeneous mixing exceeded the initial design specifications. The mixing index at the outlet of the chip was calculated to be 0.711, on a scale where 1 signifies complete mixing and 0 indicates entirely unmixed phases. This value suggests that the chip exhibits good mixing efficacy.

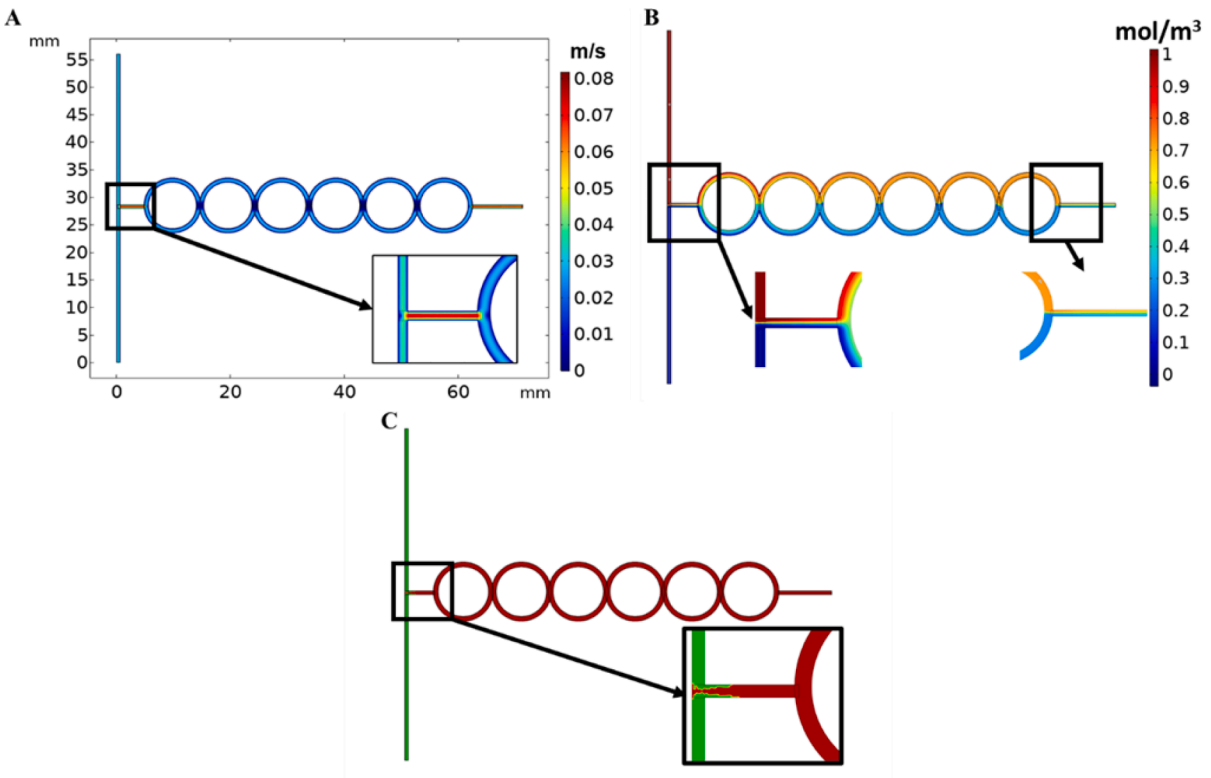

Fig. 9. Computational fluid dynamics (CFD) analysis of the 3D-printed micromixer. A. Velocity field of the micromixer calculated by CFD; **B.** Concentration gradient within the micromixer; **C.** Concentration mapping of phase distribution in the micromixer (Green field indicates at least one of the phase is not present, the red field indicates at least 1% of both phases are present.).

3.7. Particle size characterization of melatonin-SNEDDS manufactured using continuous microfluidic methods with SLA and FDM 3D-printed chips

The melatonin-loaded SNEDDS, prepared by overnight mixing method and with SLA and FDM microfluidic chips, were further diluted in deionized water and microscopically visualized using TEM. TEM images showed spherical droplets with a darker, denser core with different sizes ranging from 100 to 200 nm (Fig. 10) for all formulations.

Melatonin-loaded SNEDDS have a significantly lower particle size (one-way ANOVA, $p < 0.05$) and PDI after dilution in water compared to the melatonin cream. However, no statistically significant differences (one-way ANOVA, $p > 0.05$) were observed among the three SNEDDS manufacturing methods with similar span values (Table 4).

4. Discussion

Pre-formulation studies have shown a higher solubility of melatonin in Labrasol® (Gattefossé Labrasol Tehcnicla data sheet, 2024), a liquid surfactant of HLB 12 that consists of a small fraction of mono-, di- and triglycerides but mainly pegylated (molecular weight of 400 Da) mono- and diesters of caprylic (C8) and capric (C10) acids (Gattefosse Capryol 90 Tecnical Data Sheet, 2022). A similar length chain fatty acid was selected for the co-surfactant, Capryol® 90, which consists of propylene glycol mono- and diesters of caprylic acid. The oily vehicle that exhibited the best profile in terms of melatonin solubilization was the Labrafac® lipophile WL 1349, a mixture of medium-chain triglycerides of caprylic and capric acids. The polar heads of Labrasol® and Capryol® 90 are facing the aqueous media, while their similar length lipidic tails are oriented towards the micellar core occupied by Labrafac® lipophile

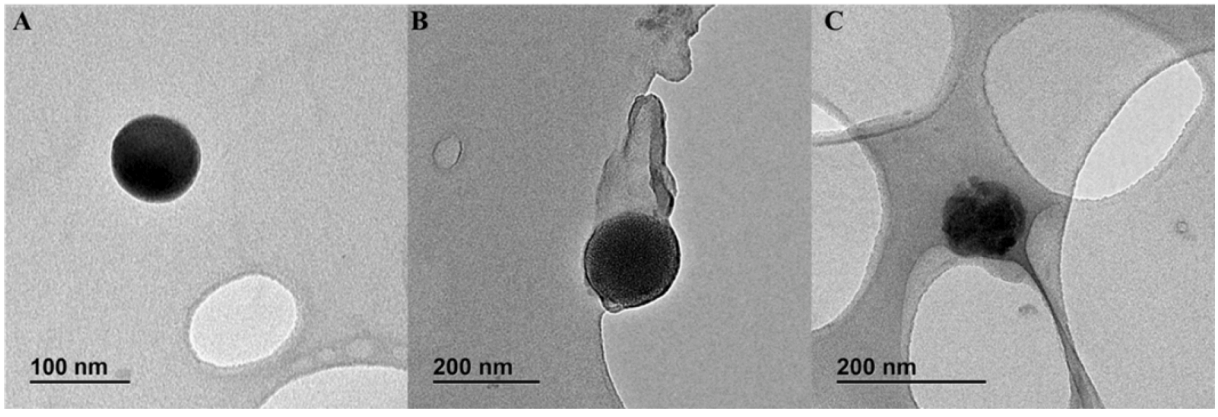

Fig. 10. Transmission electron microscopy (TEM) micrographs. A. Melatonin-loaded SNEDDS prepared by using the conventional mixing method described in section 2.2.4.; **B.** Melatonin-loaded SNEDDS prepared using the FDM microfluid chip; **C.** Melatonin-loaded SNEDDS prepared using the SLA microfluid chip.

Table 4
Particle size distribution of formulations. Key: PDI, polydispersity index.

Parameters	Melatonin Cream	Melatonin-SNEDDS	FDM chip melatonin-SNEDDS	SLA chip melatonin-SNEDDS
D_{10} (nm)	738 ± 18	65 ± 6	113 ± 12	75 ± 9
D_{50} (nm)	2,533 ± 45	102 ± 12	149 ± 18	112 ± 16
D_{90} (nm)	5,881 ± 187	192 ± 17	253 ± 34	226 ± 28
PDI	<0.1	<0.1	<0.1	<0.1
Span	2.030	1.250	0.937	1.345

Note: D10, D50, and D90 represent the particle size at which 10%, 50%, and 90% of the sample's cumulative volume are smaller than these values.

WL 1349, leading to a tighter packed micelle of smaller size (Lalatsa et al., 2020c).

Oh et al. assessed the effect of several carriers with different lipidic tail lengths on the transdermal delivery of melatonin, showing a greater permeation with the length of the lipidic tail higher for C18 followed by C16, C14 > C12, and > C10 (Oh et al., 2001). Kikwai et al. evaluated the correlation between melatonin solubility and topical permeability, showing that high solubility values do not translate to high drug permeation (Kikwai et al., 2002). In another study, isopropyl myristate, Lauroglycol® FCC, and ethanol exhibited the highest steady-state transdermal flux with 0.61, 15.85, and 156 mg/ml melatonin solubility, respectively. In our study, we have demonstrated that glycerides with a shorter tail (C8 & C10) are good solubilizers for melatonin, and the careful combination within a SNEDDS formulation results in melatonin transdermal fluxes significantly larger than those obtained with triglycerides with longer lipidic tails and other nanomedicines such as liposomes or elastic lipidic vesicles (Dubey et al., 2006).

The Stokes-Einstein equation, $D = \frac{k_B.T}{6\pi\eta r}$, states that the diffusion coefficient (D) is inversely proportional to the viscosity (η) of the medium, where k_B is the Boltzmann constant, T is the temperature, r is the particle radius (Gisladottir et al., 2009). Consequently, higher viscosity formulations may result in reduced diffusion rates, thereby decreasing permeation. Our study confirmed that lower viscosity formulations (melatonin-loaded SNEDDS) enhanced melatonin transdermal flux compared to higher viscosity melatonin cream, emphasizing the need to optimize both solubilizers and viscosity for effective delivery.

SNEDDS was optimized to achieve a droplet size of about 100 nm and formed stable nanoemulsions that are more stable in terms of droplet flocculation and coalescence (Ostwald ripening) (Anton and Vandamme, 2011; Bezerra-Souza et al., 2019). Also, formulations with a size between 50 – 150 nm have shown better permeability across the stratum corneum (Mardhiah Adib et al., 2016; Verma et al., 2003). Thus, when the optimal size is combined with a high drug loading (50 mg/g) and a fast onset of action (15 min lag time), this can allow for high levels of melatonin being able to accumulate quickly in the exposed epidermis and dermis layer for the treatment of topical wounds. SNEDDS demonstrated a linear flux over prolonged periods, which was previously observed (Lalatsa et al., 2020b; Lalatsa et al., 2020c). Other topical vehicles with lower drug loading have been reported based on Pluronic® F127 gels at 0.2 and 1.5 % (Escames et al., 2014).

Additionally, these optimized SNEDDS could be used for oral administration to treat patients exposed to CWA who suffer from mucositis, as all the excipients used are considered GRAS for the oral route. In terms of chemical stability, the melatonin-loaded SNEDDS formulation showed excellent results at 25 ℃ up to one year, which can be attributed to the H-bonds and Van der Waal forces between drug and excipients avoiding drug precipitation and also due to the lack of water in the formulation which triggers drug degradation, making it a more stable formulation compared with other topical creams or emulsions (Pranil et al., 2020). However, further experiments using an HPLC stability-indicating method should be performed to confirm the absence of any degradant.

We have demonstrated the scavenging radical capacity of the melatonin-loaded SNEDDS even in the presence of chelate ions, such as EDTA. The application of the SNEDDS can serve as a decontamination protocol for the skin after exposure to CWAs in military settings. SNEDDS will then be diluted with water on the skin after application, ensuring the formation of the nanoemulsion on the skin. Currently, the protective effect of 25 mg/g melatonin cream twice daily on breast cancer patients suffering from acute radiation dermatitis has been demonstrated (Zetner et al., 2023), but higher doses were suggested for further investigation. We were able to prepare, despite the lipophilic character of melatonin, SNEDDS with concentrations of up to 50 mg/g, which can widen the therapeutic alternatives available for clinicians and military clinicians.

Excipients used for the SNEDDS are approved for human topical use. Biocompatibility and a low risk of skin irritation have been demonstrated in rat skin models (Parveen et al., 2023), making them an excellent choice for various skin care applications (Lalatsa et al., 2020c).

In the context of military applications, SNEDDS need to be stable in harsh conditions, such as high temperatures, which may limit the use of melatonin. Alternatively, *in situ* preparation when required could facilitate their implementation as part of a decontamination protocol. SNEDDS may require lengthy mixing to ensure solubility equilibrium, which is paramount in achieving stable nanoemulsions upon emulsification with water. Zingale et al. have described a melatonin SNEDDS formulation for ocular applications using a simple mixing that resulted in nanodroplets below 50 nm and very short emulsification times (~40 s). However, Smith et al. required prolonged mixing times around 24 h to ensure full solubilization of buparvaquone in SNEDDS (Smith et al., 2018). This highlights the impact of the drug solubility in the SNEDDS on the emulsification time. Hence, enhancing the mixing efficacy can reduce the variability of the emulsification time of SNEDDS formulations. In this work, we propose an alternative mixing method based on microfluidic micromixers. In our SNEDDS formulation, the method proposed reduces the required time and can allow for a more effective mixing methodology based on the use of infusion syringe pumps and cost-effective 3D-printed micromixers. CFDs optimized T-shaped micromixers with a toroidal region. Laminar flow is characterized by low Reynolds numbers and primarily diffusion-driven mixing, although it can pose challenges for the homogenization of solutions (Stroock et al., 2002). Incorporating toroidal structures within the microfluidic device enhances mixing by generating Dean vortices and secondary flows, effectively disrupting the parabolic velocity profile characteristic of laminar flow (Zhang et al., 2019). Mixing is facilitated through the increased contact area between the drug and excipient mixture, which has a significantly higher viscosity than water. Optimizing the number of toroidal units, channel length, and channel diameter is critical to ensure optimal mixing within the microfluidic device (Kara et al., 2023).

Finally, to the best of our knowledge, this is the first report that describes a high drug-loading topical formulation containing melatonin prepared using conventional mixing as well as T-shaped toroidal micromixers that allows significant reduction in the processing time. This approach is an interesting technological advantage for military forces and potentially radiation dermatitis, considering that the formulation could be prepared at the point of care, reducing drug waste, and minimizing the risk of drug degradation upon storage.

5. Conclusions

Melatonin-loaded SNEDDS have been successfully optimized with a size of about 100 nm and enhanced loading (50 mg/g). Melatonin-SNEDDS possessed a high topical permeability, making it a promising approach for the acute treatment of skin lesions. By effectively preventing or reducing the oxidation occurring in skin lesions, this innovative formulation could significantly improve the prognosis for affected

patients. A novel continuous manufacture method for SNEDDS has been successfully implemented using a T-shaped toroidal microfluidic chip fabricated by FDM and SLA, resulting in low particle size droplets with reduced need for prolonged mixing, thereby lowering the high demands for batch quality control. While this study demonstrates the potential of microfluidic chips to yield a high quality product, the standard mixing process has not been optimized which potentially could also lead to a reduction in the preparation time of SNEDDS. This can be applied to a range of active pharmaceutical ingredients and be used as a platform processing method for a range of SNEDDS and potentially even solid SNEDDS (Kara et al., 2023; Kara et al., 2024). Additionally, the potential for further applications of 3D-printed micromixers for manufacturing at points of care medicines, such as in military bases, is demonstrated and needs to be further explored.

CRediT authorship contribution statement

Baris Ongoren: Writing – original draft, Methodology, Investigation, Formal analysis, Data curation. **Aytug Kara:** Methodology, Formal analysis, Data curation. **Luca Casettari:** Supervision, Resources, Methodology, Formal analysis. **Mattia Tiboni:** Methodology, Investigation, Formal analysis. **Aikaterini Lalatsa:** Writing – review & editing, Supervision, Data curation. **Amadeo Sanz-Perez:** Methodology, Investigation, Formal analysis. **Elena Gonzalez-Burgos:** Writing – review & editing, Supervision, Resources. **Alejandro Romero:** Writing – review & editing, Resources, Project administration, Funding acquisition. **Antonio Juberías:** Writing – review & editing, Resources, Funding acquisition, Conceptualization. **Juan J. Torrado:** Writing – review & editing, Validation, Resources, Project administration, Methodology, Funding acquisition, Conceptualization. **Dolores R. Serrano:** Writing – review & editing, Writing – original draft, Supervision, Resources, Project administration, Methodology, Investigation, Formal analysis, Data curation, Conceptualization.

Declaration of competing interest

The authors declare the following financial interests/personal relationships which may be considered as potential competing interests: [Dolores Remedios Serrano Lopez reports a relationship with Complutense University of Madrid that includes: employment].

Acknowledgements

This work has been partially funded by the University Complutense of Madrid (Research group: 910939) and the Spanish Ministry of Defense (2020/SP03390102/00000359 project). This work has been funded by the European Union – NextGenerationEU under the Italian Ministry of University and Research (MUR) National Innovation Ecosystem grant ECS00000041 - VITALITY - CUP H33C22000430006. This study has also been partially funded by the Spanish Ministry of Science and Innovation (award PID2021-126310OA-I00 to Dolores Serrano).

References

Anton, N., Vandamme, T.F., 2011. Nano-emulsions and micro-emulsions: clarifications of the critical differences. Pharm Res. 28, 978–985.
Ashrafizadeh, M., Najafi, M., Kavyiani, N., Mohammadinejad, R., Farkhondeh, T., Samarghandian, S., 2021. Anti-inflammatory activity of melatonin: a focus on the role of NLRP3 inflammasome. Inflammation 44, 1207–1222.
Bezerra-Souza, A., Fernandez-Garcia, R., Rodrigues, G.F., Bolas-Fernandez, F., Dalastra Laurenti, M., Passero, L.F., Lalatsa, A., Serrano, D.R., 2019. Repurposing butenafine as an oral nanomedicine for visceral leishmaniasis. Pharmaceutics 11.
Bezerra-Souza, A., Jesus, J.A., Laurenti, M.D., Lalatsa, A., Serrano, D.R., Passero, L.F.D., 2021. Nanoemulsified butenafine for enhanced performance against experimental cutaneous leishmaniasis. J. Immunol. Res., 8828750
Bora, N.S., Mazumder, B., Mandal, S., Bhutia, Y.D., Das, S., Karmakar, S., Chattopadhyay, P., Dwivedi, S.K., 2019. Protective effect of a topical sunscreen formulation fortified with melatonin against UV-induced photodermatitis: an immunomodulatory effect via NF-kappaB suppression. Immunopharmacol Immunotoxicol 41, 130–139.
Chen, X., Shen, J., 2017. Simulation and experimental analysis of a SAR micromixer with F-shape mixing units. Anal. Methods 9, 1885–1890.
Chobot, V., 2010. Simultaneous detection of pro- and antioxidative effects in the variants of the deoxyribose degradation assay. J. Agric. Food. Chem. 58, 2088–2094.
Chobot, V., Hadacek, F., 2011. Exploration of pro-oxidant and antioxidant activities of the flavonoid myricetin. Redox Rep. 16, 242–247.
Cruz-Hernandez, A., Roney, A., Goswami, D.G., Tewari-Singh, N., Brown, J.M., 2022. A review of chemical warfare agents linked to respiratory and neurological effects experienced in Gulf War Illness. Inhal Toxicol 34, 412–432.
Date, A.A., Desai, N., Dixit, R., Nagarsenker, M., 2010. Self-nanoemulsifying drug delivery systems: formulation insights, applications and advances. Nanomedicine (Lond) 5, 1595–1616.
Dorman, H.J., Bachmayer, O., Kosar, M., Hiltunen, R., 2004. Antioxidant properties of aqueous extracts from selected lamiaceae species grown in Turkey. J. Agric. Food Chem. 52, 762–770.
Dubey, V., Mishra, D., Asthana, A., Jain, N.K., 2006. Transdermal delivery of a pineal hormone: melatonin via elastic liposomes. Biomaterials 27, 3491–3496.
Escames, G., Acuña, D., López, L.C., 2014. Composition comprising melatonin or its derivatives with coenzyme Q10 and use thereof against ageing of the skin. Int. Patent Application No. PCT/ES2013/070817.
Fanun, M., 2007. Structure probing of water/mixed nonionic surfactants/caprylic-capric triglyceride system using conductivity and NMR. J. Mol. Liq. 133, 22–27.
Fernandez-Garcia, R., Statts, L., de Jesus, J.A., Dea-Ayuela, M.A., Bautista, L., Simao, R., Bolas-Fernandez, F., Ballesteros, M.P., Laurenti, M.D., Passero, L.F.D., Lalatsa, A., Serrano, D.R., 2020. Ultradeformable lipid vesicles localize amphotericin B in the dermis for the treatment of infectious skin diseases. ACS Infect Dis. 6, 2647–2660.
Gancitano, G., Reiter, R.J., 2022. the multiple functions of melatonin: applications in the military setting. Biomedicines 11.
Garfinkel, D., Laudon, M., Nof, D., Zisapel, N., 1995. Improvement of sleep quality in elderly people by controlled-release melatonin. Lancet 346, 541–544.
Gattefosse Capryol 90 Technical Data Sheet. Available at: https://www.gattefosse.com/pharmaceuticals-products/capryol-90. Accessed date: 1 september 2023.
Gattefossé Labrasol Technical data sheet. Available at. https://www.gattefosse.com/pharmaceuticals/product-finder/labrasol. Accessed date: 30 April 2024.
Gisladottir, S., Loftsson, T., Stefansson, E., 2009. Diffusion characteristics of vitreous humour and saline solution follow the Stokes Einstein equation. Graefes Arch. Clin. Exp. Ophthalmol 247, 1677–1684.
Gulcin, I., Buyukokuroglu, M.E., Kufrevioglu, O.I., 2003. Metal chelating and hydrogen peroxide scavenging effects of melatonin. J. Pineal. Res. 34, 278–281.
Gutteridge, J.M.C., 1994. Biological origin of free radicals, and mechanisms of antioxidant protection. Chem. Biol. Interact. 91, 133–140.
Javaid, M.U., Cheema, T.A., Park, C.W., 2018. Analysis of passive mixing in a serpentine microchannel with sinusoidal side walls. Micromachines 9, 8.
Kara, A., Ongoren, B., Anaya, B.J., Lalatsa, A., Serrno, D.R., (2024). Continuous Microfluidic Manufacture of Nano-in-Microparticles combining 3D-printed Micromixers and Spray Drying.
Kara, A., Vassiliadou, A., Ongoren, B., Keeble, W., Hing, R., Lalatsa, A., Serrano, D.R., 2021. Engineering 3D printed microfluidic chips for the fabrication of nanomedicines. Pharmaceutics 13.
Kara, A., Kumar, D., Healy, A.M., Lalatsa, A., Serrano, D.R., 2023. Continuous manufacturing of cocrystals using 3D-printed microfluidic chips coupled with spray coating. Pharmaceuticals 16, 1064.
Kaur, L., Singh, K., Paul, S., Singh, S., Singh, S., Jain, S.K., 2018. A mechanistic study to determine the structural similarities between artificial membrane strat-M and biological membranes and its application to carry out skin permeation study of amphotericin B nanoformulations. AAPS PharmSciTech.
Kehe, K., Szinicz, L., 2005. Medical aspects of sulphur mustard poisoning. Toxicology 214, 198–209.
Kikwai, L., Kanikkannan, N., Babu, R.J., Singh, M., 2002. Effect of vehicles on the transdermal delivery of melatonin across porcine skin in vitro. J. Control Release 83, 307–311.
Kleszczynski, K., Zillikens, D., Fischer, T.W., 2016. Melatonin enhances mitochondrial ATP synthesis, reduces reactive oxygen species formation, and mediates translocation of the nuclear erythroid 2-related factor 2 resulting in activation of phase-2 antioxidant enzymes (gamma-GCS, HO-1, NQO1) in ultraviolet radiation-treated normal human epidermal keratinocytes (NHEK). J. Pineal Res. 61, 187–197.
Lalatsa, A., Emeriewen, K., Protopsalti, V., Skelton, G., Saleh, G.M., 2016. Developing transcutaneous nanoenabled anaesthetics for eyelid surgery. Br. J. Ophthalmol. 100, 871–876.
Lalatsa, A., Patel, P.V., Sun, Y., Kiun, C.C., Karimi, F., Zekonyte, J., Emeriewen, K., Saleh, G.M., 2020. Transcutaneous anaesthetic nano-enabled hydrogels for eyelid surgery. Int. J. Pharm. 577, 119003.
Lalatsa, A., Statts, L., Adriana de Jesus, J., Adewusi, O., Auxiliadora Dea-Ayuela, M., Bolas-Fernandez, F., Dalastra Laurenti, M., Passero L, F.D., Serrano, D.R., 2020c. Topical buparvaquone nano-enabled hydrogels for cutaneous leishmaniasis. Int. J. Pharm. 588, 119734.
Mardhiah Adib, Z., Ghanbarzadeh, S., Kouhsoltani, M., Yari Khosroshahi, A., Hamishehkar, H., 2016. The effect of particle size on the deposition of solid lipid nanoparticles in different skin layers: a histological study. Adv. Pharm. Bull 6, 31–36.
Milani, M., Sparavigna, A., 2018. Antiaging efficacy of melatonin-based day and night creams: a randomized, split-face, assessor-blinded proof-of-concept trial. Clin. Cosmet. Investig. Dermatol. 11, 51–57.

Milano, M., Puviano, M., 2018. Anti-aging efficacy of melatonin-based cream: clinical and instrumental skin evaluation. Cosmetics 5, 1–7.
Monograph, M., (2023). Melatonin Monograph. United States Pharmacopeia, Docid: GUID-454646BE-F1DF-458C-9011-1FBBCCEFE5BC_4_en-US, 2023.
Montenegro, L., 2017. Lipid-based nanoparticles as carriers for dermal delivery of antioxidants. Curr. Drug Metab. 18, 469–480.
Oh, H.J., Oh, Y.K., Kim, C.K., 2001. Effects of vehicles and enhancers on transdermal delivery of melatonin. Int. J. Pharm. 212, 63–71.
Pandi-Perumal, S.R., Srinivasan, V., Maestroni, G.J., Cardinali, D.P., Poeggeler, B., Hardeland, R., 2006. Melatonin: Nature's most versatile biological signal? FEBS J. 273, 2813–2838.
Parveen, N., Sheikh, A., Molugulu, N., Annadurai, S., Wahab, S., Kesharwani, P., 2023. Drug permeation enhancement, efficacy, and safety assessment of azelaic acid loaded SNEDDS hydrogel to overcome the treatment barriers of atopic dermatitis. Environ. Res. 236, 116850.
Pita, R., Marco-Contelles, J., Ramos, E., Del Pino, J., Romero, A., 2013. Toxicity induced by chemical warfare agents: insights on the protective role of melatonin. Chem. Biol. Interact. 206, 134–142.
Pita, R., Vidal-Asensi, S., 2010. Cutaneous and systemic toxicology of vesicants used in warfare. Actas Dermosifiliogr 101, 7–18.
Pranil, T., Moongngarm, A., Loypimai, P., 2020. Influence of pH, temperature, and light on the stability of melatonin in aqueous solutions and fruit juices. Heliyon 6, e03648.
Reiter, R.J., Tan, D.X., Galano, A., 2014. Melatonin: exceeding expectations. Physiology (Bethesda) 29, 325–333.
Rice, P., 2003. Sulphur mustard injuries of the skin. Pathophysiology and Management. Toxicol Rev. 22, 111–118.
Rodriguez Fernandez, M.J., Serrano Lopez, D.R., Torrado, J.J., 2022. Effect of primary packaging material on the stability characteristics of diazepam and midazolam parenteral formulations. Pharmaceutics 14.
Romero, A., Ramos, E., Lopez-Muñoz, F., de los Ríos, C., Egea, J., Gil-Martín, E., Pita, R., Torrado, J.J., Serrano, D.R.A.J., 2021. Toxicology of blister agents: is melatonin a potential therapeutic option? Diseases 9, 1–16.
Sekkin, S., Ipek, E., Boyacioglu, M., Kum, C., Karademir, U., Hande, Y., Mehmet, A., Hulki, B., 2015. DNA protective effects of melatonin on oxidative stress in streptozotocin - induced diabetic rats. Front. Genet. 6.
Serrano, D.R., Gordo, M.J., Matji, A., Gonzalez, S., Lalatsa, A., Torrado, J.J., 2019. Tuning the transdermal delivery of hydroquinone upon formulation with novel permeation enhancers. Pharmaceutics 11.
Shokrzadeh, M., Naghshvar, F., Ahmadi, A., Chabra, A., Jeivad, F., 2014. The potential ameliorative effects of melatonin against cyclophosphamide-induced DNA damage in murine bone marrow cells. Eur. Rev. Med. Pharmacol. Sci. 18, 605–611.
Strat-M® Membrane for Transdermal Diffusion Testing. Available at: https://www.merckmillipore.com/ES/es/product/Strat-M-Membrane-for-Transdermal-Diffusion-Testing,MM_NF-C112892. Accessed date: 1 September 2023.
Stroock, A.D., Dertinger, S.K., Ajdari, A., Mezic, I., Stone, H.A., Whitesides, G.M., 2002. Chaotic mixer for microchannels. Science 295, 647–651.
Ta, B.Q., Le Thanh, H., Dong, T., Thoi, T.N., Karlsen, F., 2015. Geometric effects on mixing performance in a novel passive micromixer with trapezoidal-zigzag channels. J. Micromech. Microeng. 25, 094004.
Tekbas, O.F., Ogur, R., Korkmaz, A., Kilic, A., Reiter, R.J., 2008a. Melatonin as an antibiotic: new insights into the actions of this ubiquitous molecule. J. Pineal Res. 44.
Tekbas, O.F., Ogur, R., Korkmaz, A., Killic, A., Reiter, R.J., 2008b. Melatonin as an antibiotic: new insights into the actions of this ubiquitous molecule. J. Pineal. Res 44.
Tiboni, M., Tiboni, M., Pierro, A., Del Papa, M., Sparaventi, S., Cespi, M., Casettari, L., 2021. Microfluidics for nanomedicines manufacturing: an affordable and low-cost 3D printing approach. Int. J. Pharm. 599, 120464.
Verma, D.D., Verma, S., Blume, G., Fahr, A., 2003. Particle size of liposomes influences dermal delivery of substances into skin. Int J Pharm 258, 141–151.
Zetner, D., Kamby, C., Christophersen, C., Gulen, S., Paulsen, C.B., Piga, E., Hoffmeyer, B., Mahmood, F., Rosenberg, J., 2023. Effect of melatonin cream on acute radiation dermatitis in patients with primary breast cancer: a double-blind, randomized, placebo-controlled trial. J. Pineal Res. 75, e12873.
Zhang, C., Ferrell, A.R., Nandakumar, K., 2019. Study of a toroidal-helical pipe as an innovative static mixer in laminar flows. Chem. Eng. J. 359, 446–458.
Zhang, H.-M., Zhang, Y., 2014. Melatonin: a well-documented antioxidant with conditional pro-oxidant actions. J. Pineal Res. 57, 131–146.
Zingale, E., Bonaccorso, A., D'Amico, A.G., Lombardo, R., D'Agata, V., Rautio, J., Pignatello, R., 2024. Formulating resveratrol and melatonin self-nanoemulsifying drug delivery systems (SNEDDS) for ocular administration using design of experiments. Pharmaceutics 16, 125.